MNRAS 000, 1–7 (2015) Preprint 9 September 2019 Compiled using MNRAS LATEX style file v3.0

Matter power spectrum: from Lyα forest to CMB scales

Solène Chabanier[1]★, Marius Millea[2,3,4], Nathalie Palanque-Delabrouille[1]

[1] *IRFU, CEA, Université Paris-Saclay, F91191 Gif-sur-Yvette, France*
[2] *Berkeley Center for Cosmological Physics, LBNL and University of California at Berkeley, Berkeley, California 94720, USA*
[3] *Institut d'Astrophysique de Paris (IAP), UMR 7095, CNRS-UPMC Université Paris 6, Sorbonne Universités, 98bis boulevard Arago, F-75014 P*
[4] *Institut Lagrange de Paris (ILP), Sorbonne Universités, 98bis boulevard Arago, F-75014 Paris, France*

Accepted 2019 August 10. Received 2019 August 9; in original form 2019 May 22

ABSTRACT

We present a new compilation of inferences of the linear 3D matter power spectrum at redshift $z = 0$ from a variety of probes spanning several orders of magnitude in physical scale and in cosmic history. We develop a new lower-noise method for performing this inference from the latest Lyα forest 1D power spectrum data. We also include cosmic microwave background (CMB) temperature and polarization power spectra and lensing reconstruction data, the cosmic shear two-point correlation function, and the clustering of luminous red galaxies. We provide a Dockerized Jupyter notebook housing the fairly complex dependencies for producing the plot of these data, with the hope that groups in the future can help add to it. Overall, we find qualitative agreement between the independent measurements considered here and the standard ΛCDM cosmological model fit to the *Planck* data.

Key words: cosmology: observations – (cosmology:) large-scale structure of Universe

1 INTRODUCTION

The ΛCDM model provides a simple and remarkable fit to much of the existing cosmological data, forming the basis of the standard cosmological paradigm. The cosmic microwave background (CMB) temperature and polarization anisotropies observed by the *Planck* satellite can be explained with only the six free parameters of the ΛCDM model (Planck Collaboration et al. 2018; Collaboration et al. 2018a). In this paper, we illustrate the extent to which this model, with parameters fixed to their best-fit given *Planck* data, is in agreement with a number of other probes spanning cosmic time and cosmic scales. In an initial work, Tegmark & Zaldarriaga (2002) demonstrated the consistency between the ΛCDM model fit to the WMAP CMB data (Bennett et al. 2013), the first iteration of the Sloan Digital Sky Survey (SDSS I) (York et al. 2000) clustering data that were available at the time, the 2 Degree Field Galaxy redshift Survey(2dFGRS) (Colless et al. 2001) galaxy clustering data and the Red-Sequence Cluster Survey (Hoekstra et al. 2002) weak lensing data. More recent updates to this work include Tegmark & Zaldarriaga (2009) and Hlozek et al. (2012), which included newer data and other types of probes. With the advent of the Planck mission, of the third and fourth iterations of the Sloan Digital Sky Survey (Blanton et al. 2017) and of the Dark Energy Survey (The Dark Energy Survey Collaboration 2005), the measurements have now reached an improvement of about an order of magnitude in precision over the last two decades since the initial work. These updated data sets make it timely to reevaluate the overall agreement.

The main results of the paper are two-fold. First, focusing in particular on the Lyα constraints, we develop a new more accurate method for processing these data into a constraint on the linear matter power spectrum, $P_{\rm m}(k)$, at redshift zero. This method is based on a technique known as total variation regularization (TVR; Chartrand 2005), which reduces noise in the resulting estimate. Second, we take this constraint, combined with a number of others, and produce a compilation of $P_{\rm m}(k)$, shown in Fig. 1. On scales of a few Mpc, we include the information embedded in the Lyα forest measured with the quasar survey of the SDSS IV fourteenth data release (Abolfathi et al. 2018). Partially overlapping in scale, we also use the cosmic shear measurement from the DES YR1 data release (Troxel et al. 2017). On scales of several tens of Mpc, we use the power spectrum of the halo density field derived from a sample of luminous red galaxies (LRG) from the SDSS seventh data release (DR7) (Reid et al. 2010). Finally, on the largest scales, we use the anisotropies of the microwave background measured by the Planck satellite. In addition to probing a wide range of scales, from $k = 2 \times 10^{-4}$ to $k = 2\,h\,\mathrm{Mpc}^{-1}$, these data also

★ E-mail: solene.chabanier@cea.fr

cover a large range of cosmic epochs: $z \sim 0.35$ for the LRG, $z \sim 0.2$ to 1.3 for the shear measurements, $z = 2.2$ to 4.6 for the more distant Lyα forest, and $z \sim 10^3$ for CMB.

As described in Tegmark & Zaldarriaga (2002), inferring the linear matter spectrum at $z = 0$ from the various probes we consider here is a highly model-dependent process. We take as our fiducial model the Planck 2018 best-fit ΛCDM model (Planck Collaboration et al. 2018). The results here are therefore a test of the consistency of this model, rather than direct constraints on the matter power spectrum. In general, we find qualitative agreement of this fiducial model with the data we consider.

The datasets which we consider were chosen to be representative of different types of cosmological measurements which exist and to cover a broad range of scales, particularly favoring ones where data products were especially convenient for the calculations we perform here. Of course, many other measurements exist which provide constraints on the matter power spectrum, some of which are known to be in varying degrees of tension with the *Planck* best-fit model. It is beyond the scope of this work to include them all, however we provide a Dockerized Jupyter notebook which includes the fairly complex dependencies needed to produce this plot. We hope that this makes it easy for any group in the future to add any desired data set and keep up-to-date this compilation. The repository for this notebook can be found here: [1].

The outline of the paper is as follows. In Sec. 2, we present the Lyα data and explain how we compute the 3D matter power spectrum from the published 1D flux power spectrum. These data are the ones whose treatment differs the most from the previous study of Croft et al. (2002) used in Tegmark & Zaldarriaga (2002). In Sec. 3, we present the other probes we use (CMB, cosmic shear and galaxy clustering) and the general method we apply to compute the 3D matter power spectrum in each case. We conclude in Sec. 4.

2 MATTER POWER SPECTRUM FROM THE LYMAN-ALPHA FOREST

2.1 Lyman-alpha data

With the advent of medium-resolution spectroscopic surveys that increased by several orders of magnitude the number of spectroscopically observed high-redshift quasars, the past decade has witnessed a significant ramp up of the use of Lyα forest as a cosmological probe. The Sloan Digital Sky Survey in particular, with the BOSS and eBOSS surveys (Dawson et al. 2016; Blanton et al. 2017), has now observed over two hundred thousand quasar spectra at redshifts above 2.1. The 3D correlations in the Lyα flux transmission field were studied extensively in Slosar et al. (2011); Busca et al. (2013); Slosar et al. (2013); Kirkby et al. (2013); Delubac et al. (2015); Bautista et al. (2017) to measure the position of the Baryon Acoustic Oscillation peak and provide constraints on dark matter and dark energy. The correlations along the line of sight provide information on smaller scales. The 1D flux power spectrum measured from the Lyα data, for instance, is a remarkable probe of the impact on structure formation of neutrino masses (Palanque-Delabrouille et al. 2015a,b; Yèche et al. 2017), of warm dark matter (Baur et al. 2016; Iršič et al. 2017; Armengaud et al. 2017) or of various models of sterile neutrinos (Baur et al. 2016, 2017).

In this work, we use data from the eBOSS DR14 release (Abolfathi et al. 2018), corresponding to the entirety of the BOSS survey complemented by the first year of eBOSS. We take the 1D transmitted flux power spectrum measured by the BOSS and eBOSS collaborations in Chabanier et al. (2018). It used a selection of 43,751 highest-quality quasar spectra from a parent sample of 180,413 visually inspected spectra. They were selected for the absence of BAL features, a good mean spectral resolution and high mean signal-to-noise ratio per pixel. The analysis gives the flux power spectrum along a line of sight, $P_{\rm tot\,1D}$, in thirteen equally-spaced redshift bins covering the range $z = 2.2$ to 4.6 with $\Delta z = 0.2$. The highest redshift bin is built from 63 quasars only and has large uncertainties. We therefore use only the lowest twelve redshift bins in this work. These data show an oscillatory feature due to the correlated absorption by Lyα and SiIII at a velocity separation $\Delta v = 2271$ km.s^{-1}. Adopting the approach from McDonald et al. (2006), we model the total transmission flux fraction as,

$$\delta_{\rm tot} = \delta(v) + a\delta(v + \Delta v), \tag{1}$$

with $\delta(v)$ being only for Lyα. The resulting power spectrum is

$$P_{\rm tot\,1D}(k) = (1 + a^2)P_{F1D}(k) + 2a\cos(\Delta v\, k)P_{F1D}(k) \tag{2}$$

We use equation 2 to correct for these wiggles, where a is fit independently for each redshift bin. We use these 1D transmitted flux power spectra to derive the 3D matter power spectrum as explained below.

2.2 Method

We follow the prescription of Croft et al. (1998), updated in Croft et al. (2002). We assume that the 3D flux power spectrum P_{F3D} is related to the linear matter power spectrum $P_{\rm m}$ by a proportionality relation,

$$P_{\rm m}(k, z) = \frac{P_{F3D}(k, z)}{b^2(k, z)}\,, \tag{3}$$

with $b(k, z)$ a scale and redshift dependent bias that depends on the cosmological model. The scale dependence is an improvement over the initial methodology, added in Croft et al. (2002), to take into account the effects of non-linear evolution, thermal broadening and peculiar velocities.

The 1D and the 3D flux power spectra are related by

$$P_{F3D}(k) = -\frac{2\pi}{k}\frac{{\rm d}P_{F1D}(k)}{{\rm d}k}\,, \tag{4}$$

which we use to derive the 3D flux power spectrum needed in Eq. (3).

We compute the bias $b(k, z)$ for each of the twelve redshift bins mentioned above using CAMB[2]. The simulations are produced for a grid of parameters whose values are varied

[1] https://github.com/marius311/mpk_compilation

[2] https://camb.info (Lewis et al. 2000) for the linear matter power spectrum, and hydrodynamic simulations dedicated to the analysis of the BOSS 1D data (Borde et al. 2014) for the 1D flux power spectrum

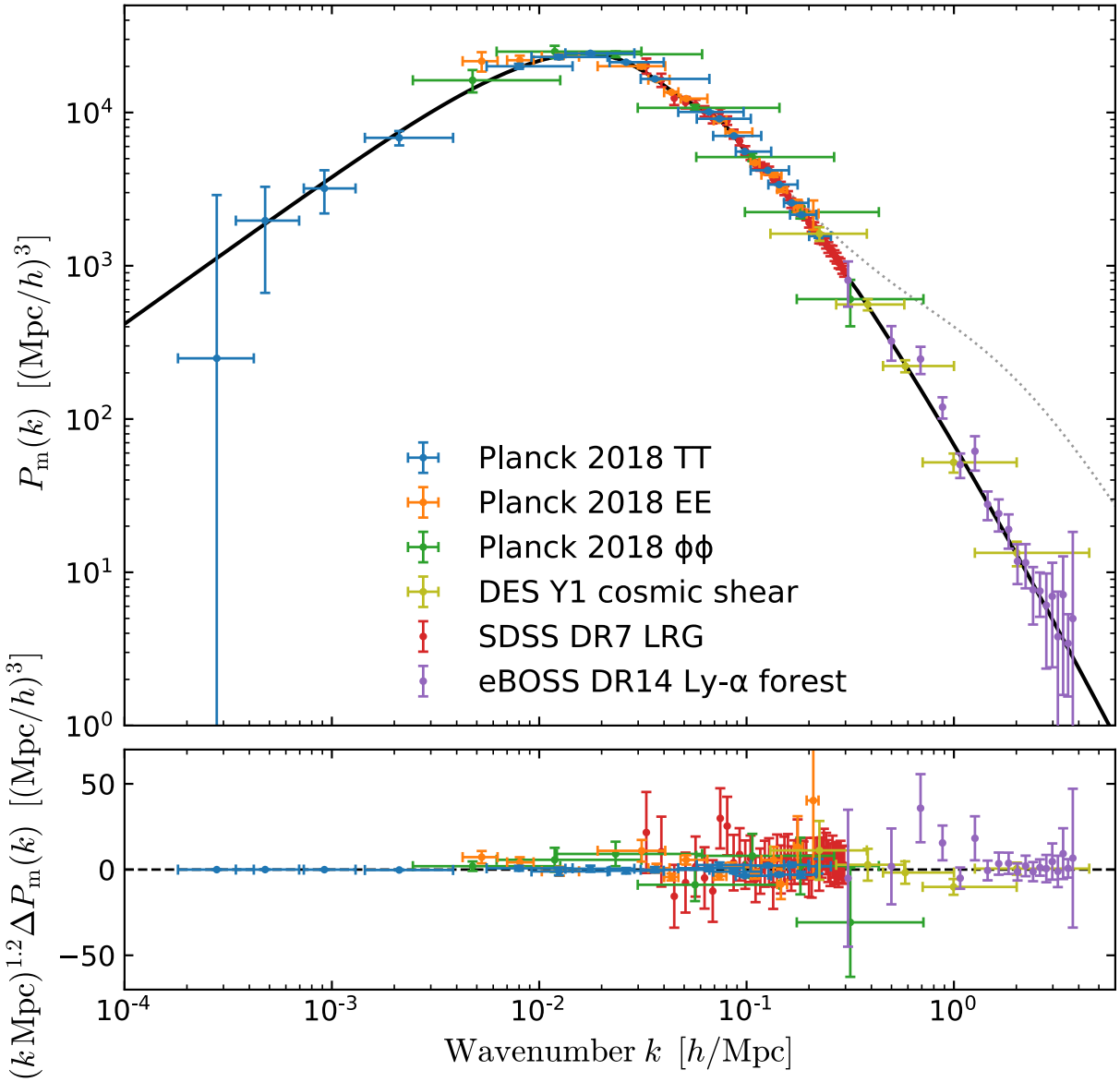

Figure 1. *Top*: Data points show inferences of the 3D linear matter power spectrum at $z = 0$ from Planck CMB data on the largest scales, SDSS galaxy clustering on intermediate scales, SDSS Lyα clustering and DES cosmic shear data on the smallest scales. In cases where error bars in the k-direction are present, we have used the method of Tegmark & Zaldarriaga (2002) to calculate a central 60% quantile of the region to which each data point is sensitive. In other cases, data points represent the median value of the measurement. The solid black line is the theoretical expectation given the best-fit *Planck* 2018 ΛCDM model (this model also enters the computation of the data points themselves). The dotted line for reference shows the theoretical spectrum including non-linear effects. *Bottom*: deviation of the data from the Planck best fit ΛCDM 3D matter power spectrum.

around a central model. The four cosmological parameters are the scalar spectral index n_s, the RMS matter fluctuations amplitude today in linear theory σ_8, the matter density today Ω_m, and the expansion rate today H_0. The astrophysical parameters (all at $z = 3$) are the normalization temperature of IGM T_0, the logarithmic slope of the δ dependence of the IGM temperature γ, the effective optical depth of the Lyα absorption A^τ and the logarithmic slope η^τ of the redshift dependence of A^τ. The central (also dubbed best-guess) simulation is based upon a fiducial model corresponding to the Planck Collaboration et al. (2014) best-fit cosmology. The simulation grid, however, allows us to test other cosmologies.

In Table 1, we list the values of the parameters used in the best-guess simulation, as well as the corresponding

Table 1. Fit parameters. First column: central value and variation range in the simulation grid. Second column: best-fit value and 68% confidence interval for a fit to Lyα + Planck (TT + lowE).

Parameter	Simulations	Best-fit
n_s	0.96 ± 0.05	0.954 ± 0.004
σ_8	0.83 ± 0.05	0.817 ± 0.007
Ω_m	0.31 ± 0.05	0.330 ± 0.009
H_0 $(km.s^{-1}.Mpc^{-1})$	67.5 ± 5	66.2 ± 0.6
$T_0(z=3)$ (K)	14000 ± 7000	11300 ± 1600
$\gamma(z=3)$	1.3 ± 0.3	0.7 ± 0.1
A^τ	0.0025 ± 0.0020	0.0026 ± 0.0001
η^τ	3.7 ± 0.4	3.734 ± 0.015

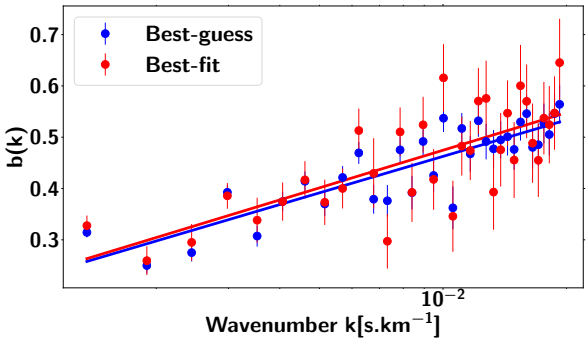

Figure 2. Biases computed at $z = 2.8$ for the best-guess (in blue) and best-fit (in red) configurations. The lines are linear-log fits to each case.

best-fit values measured in Chabanier et al. (2018), for a fit to the eBOSS 1D Lyα power spectrum combined with the Planck 2018 "TT+lowE" likelihood (Planck Collaboration et al. 2018). The best-fit model is in good agreement with the central simulation. The parameters that deviate the most from their central value are σ_8 and Ω_m. We determine the biases $b_{\rm bf}$ for the best-fit model by computing the biases $b_{\rm bg}$ for the best-guess simulation, and we apply first-order corrections to account for the measured shifts in σ_8 and Ω_m, using simulations where all parameters are kept to their central value except for either σ_8 or Ω_m. We determine the bias $b(z,k)$ at each redshift z and scale k by

$$b_{\rm bf}(z,k) = b_{\rm bg}(z,k) + (\sigma_{8,\rm bf} - \sigma_{8,\rm bg})\frac{{\rm d}b}{{\rm d}\sigma_8}(\sigma_{8,\rm bg}, \Omega_{m,\rm bg}) + (\Omega_{m,\rm bf} - \Omega_{m,\rm bg})\frac{{\rm d}b}{{\rm d}\Omega_m}(\sigma_{8,\rm bg}, \Omega_{m,\rm bg})\,.$$

Fig. 2 shows both best-guess and best-fit biases for redshift $z = 2.8$. As illustrated in the figure for a specific redshift, but similarly for all redshifts, the linear corrections have little effect.

Eq. (3) thus allows us compute the linear power spectra $P_{\rm m}(k, z_i)$ for all twelve redshift bins z_i. We then transpose each of them to $z = 0$ with the relation

$$P_{{\rm m},z_i}(k,0) = P_{\rm m}(k,z_i) \times t(k,z_i)\,, \quad (5)$$

where the evolution term $t(k, z_i)$ is determined in linear theory using a Boltzmann code such as CAMB[3] (Lewis et al. 2000) or CLASS[4] (Lesgourgues 2011). Finally we combine all twelve $z = 0$ power spectra $P_{{\rm m},z_i}$ using an inverse-variance weighted average. The top panel of Fig. 3 shows the resulting $P_{\rm m}(k, 0)$.

2.3 Total Variation Regularization

The discrete differentiation of the 1D transmitted flux power spectrum P_{F1D} to obtain the 3D transmitted flux power spectrum P_{F3D} significantly amplifies noise and uncertainties. The effect is worst at small scales where only the highest redshift bins, which are also the noisiest, contribute to the measurement. To reduce this computational artifact, we use a refined differentiating technique, the total variation regularization (TVR) method, proposed in Chartrand (2005). It is a specific regularization process that estimates the derivative of a function f as the minimizer u_{min} of the functional F,

$$F(u) = \alpha R(u) + DF(Au - f), \quad (6)$$

where α is the regularization parameter, $R(u)$ is the regularization term which penalizes noise, and $DF(Au - f)$ is the data fidelity term with $Au(x) = \int_0^x u$. The TVR uses $R(u) = \int |u'|$ and $DF(\cdot) = \int |\cdot|^2$. The resulting algorithm has only one free parameter, α, that we fix to 10^{-5} for all the redshift bins, as it appears to be a good compromise between smoothing the data and conserving valuable information. We tested the TVR on an analytical form of the 1D flux power spectrum, which allowed us to compare the resulting derivative to the true P_{F3D}. The TVR induces no computational bias, except on the first three sampling points, which we hence decide not to keep in the following. To estimate the uncertainty on the 3D power spectrum resulting from this regularization, we perform a parametric bootstrap at each k bin with 1000 iterations. The bottom panel of Fig. 3 shows the final 3D matter power spectrum at redshift $z = 0$ derived with the TVR approach. The dispersion is clearly reduced and the power spectrum from TVR considerably smoother than the one from a straight derivative. The TVR technique increases the correlations between neighboring points (up to 50% in the worst case, for nearest-neighbor correlation), although correlations with next-to-nearest neighbors are between 1 and 20% at most.

Finally, we point out that we use the TVR derivation for the data but we keep to straight derivatives to compute the biasing functions from the hydrodynamic simulations. The reason is the following. The P_{F1D} from the simulations is much smoother than in the data, and systematic uncertainties from the bias term are largely sub-dominant compared to data statistical uncertainties. Using the TVR technique on the simulations would therefore unnecessarily increase the correlations between neighboring points without yielding a measurable gain on the resulting uncertainties.

[3] https://camb.info
[4] http://class-code.net/

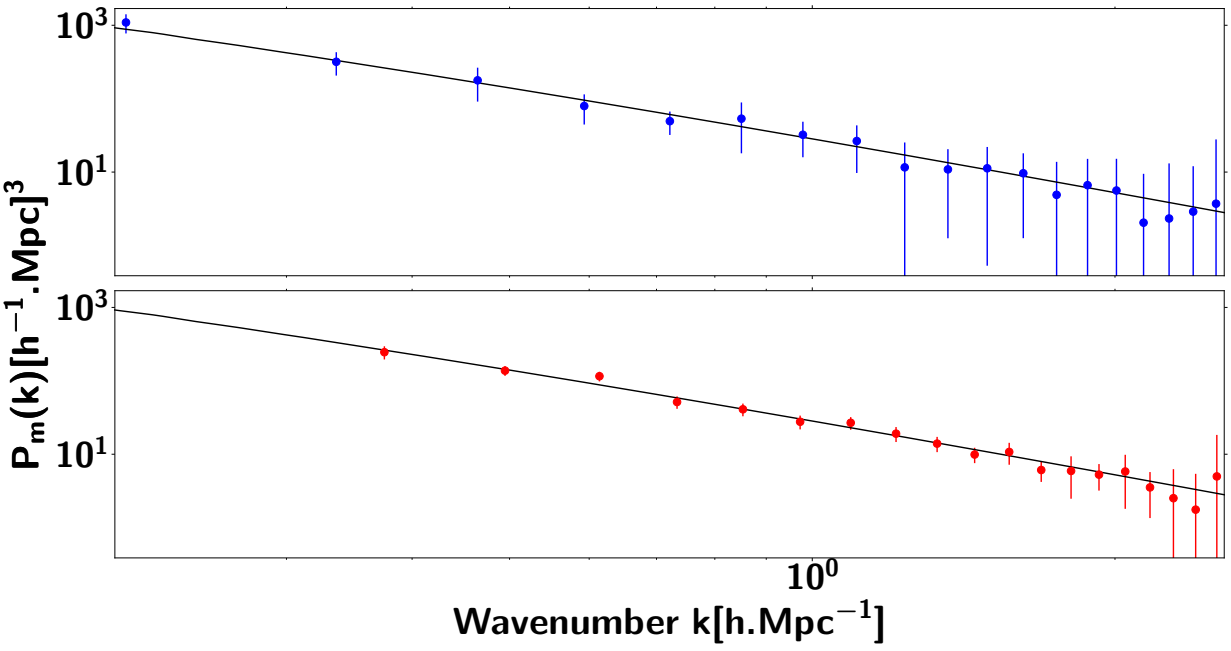

Figure 3. Linear matter power spectrum inferred from Lyα data. Results from the discrete differentiation are shown in the top panel, and from the TVR approach in the bottom panel. The black solid line is the linear theory expectation.

3 MATTER POWER SPECTRUM FROM OTHER PROBES

Having described in some detail the Lyα forest constraints and our new TVR-based method for calculating them, we now turn to constraints from the other datasets considered in this work, which more closely follow the procedure laid out by Tegmark & Zaldarriaga (2002). Their procedure is based on the relating a given observable, d_i (which can be for example a CMB C_ℓ, or measurement of cosmic shear power spectrum at some redshift, etc...), to $P_{\rm m}(k,0)$, via

$$d_i = \int d\ln k\, W_i(k) P_{\rm m}(k,0) \tag{7}$$

Each given observable will have a different "window" function, $W_i(k)$, which can be calculated from theory for a fixed cosmological model. In many cases, for example if our d_i are simple auto-correlation functions, the $W_i(k)$ are strictly positive. Furthermore, depending on the exact quantity measured, they are often also fairly localized in k. In these cases, we normalize the $W_i(k)$ to unit area, effectively treating it as a probability distribution, and, following Tegmark & Zaldarriaga (2002), take the error bar in the k-direction in Fig. 1 to denote the middle 80% quantile of this distribution. Our slight modification to their procedure is that whereas they take the middle 80% of the quantity $W_i(k)P_{\rm m}(k,0)$, we take it of just $W_i(k)$. We view this as the more natural choice since it is just $W_i(k)$ which represents the projection of the data into the redshift zero matter power spectrum. Additionally, this gives us a k-direction error bar which does not depend on the shape of $P_{\rm m}(k,0)$.

In Fig. 4, we plot the window functions for the different observations which we use. In each case, some "rebinning" of the data is applied as compared to the raw data products provided by each experiment. This is done so as to produce more reasonably spaced data points in the k direction, and to improve the localization of the $W_i(k)$. We describe these rebinnings in the individual sections below. One can verify the localized nature of the different window functions, indicating the validity of interpreting each data point as a constraint on $P_{\rm m}(k,0)$.

Cosmic microwave background For CMB data, we use the *Planck* 2018 temperature, polarization, and lensing reconstruction power spectra (Collaboration et al. 2018a,b). At $\ell < 30$ in temperature, we use the C_ℓ's provided by the Commander likelihood, with the asymmetric errorbars averaged together, which should have minimal impact as we also bin multiple C_ℓ's together which will have a symmetrizing effect. At $\ell > 30$ in temperature and polarization, we use the Plik-like bandpowers and covariance, rebinned as described above. We do not use polarization below $\ell < 30$ because the signal there is highly reionization-model dependent (e.g., Zaldarriaga 1997). For the lensing reconstruction, we use the bandpowers and covariance from the "agressive" data cut. The window functions are shown in Fig. 4. One can see that the TE window functions are not strictly positive since they do not arise from an auto spectrum. For this reason, we cannot interpret them as a constraint on the amplitude of $P_{\rm m}(k,0)$, hence we show only TT and EE in Fig. 1. Although we do not do so here, one could interpret them as a constraint on a linear combination of the amplitude and derivative of $P_{\rm m}(k,0)$, however.

Cosmic shear For cosmic shear, we use DES first-year

constraints on the cosmic shear real-space two-point correlation functions $\xi_{\pm}^{ij}(\theta)$, where the i and j indices label different redshift bins (Troxel et al. 2017). These functions can be written in the form of Eq. (7),

$$\xi_{\pm}^{ij}(\theta) = \int d\ln k\ W_{\pm}^{ij}(\theta, k) P(k, 0), \tag{8}$$

where

$$W_{\pm}^{ij}(\theta, k) = \frac{1}{2\pi} \int_0^{\chi^H} d\chi\ \ell(\ell + 1/2) J_{0/4}(\theta\ell) \frac{q^i(\chi) q^j(\chi)}{\chi^2} \frac{P(k, \chi)}{P(k, 0)}, \tag{9}$$

the $q^i(\chi)$ are the lensing efficiency functions defined as usual (e.g. as in Troxel et al. 2017), and

$$k = \frac{\ell + 1/2}{\chi}. \tag{10}$$

We choose to bin together all of the redshift bins, producing a set of 5 fairly localized window functions for each θ bin, plotted in Fig. 4. Interestingly, one can see that ξ_+ produces window functions which are not strictly positive. This arises due to the weighting of the Bessel function inside of the integrand. Thus, similarly as for the CMB TE power spectrum, we do not plot these constraints on Fig. 1, although they could in theory also be interpreted as a joint constraint on the amplitude and derivative.

Galaxy clustering For galaxy clustering, we use measurements of the halo power spectrum from a sample of luminous red galaxies from the Sloan Digital Sky Survey seventh data release (Reid et al. 2010). Using a model for the halo bias, we can relate these measurements to the underlying linear matter power spectrum in which we are interested. We use the model given in Reid et al. (2010) with free parameters b_0, a_1, and a_2. Fitting to our fiducial cosmological model, we find best-fit values of $1.24, 0.54$, and -0.33, respectively, at a pivot scale of $k_\star = 0.2\,\mathrm{Mpc}/h$.

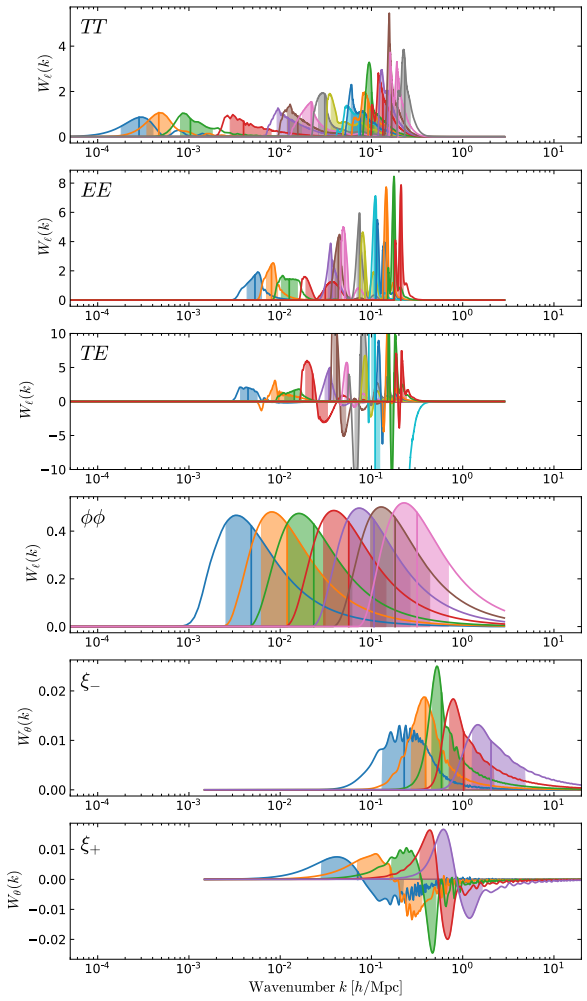

Figure 4. The window functions, $W_i(k)$, for several of the datasets considered here. The shaded region represents the middle 80% quantile of the absolute value of the function, which is the region denoted by the k-direction error bars in Fig. 1, and represents roughly to which k-scales a given data observation is sensitive to. Note that some observations have non-strictly positive windows, meaning we cannot interpret them as simply a measure of the overall amplitude of the matter power spectrum at a given scale, but rather some combination of this and its derivative.

4 CONCLUSIONS

In this letter, we present a measurement of the 3D matter power spectrum at redshift $z = 0$ by combining different cosmological probes spanning four orders of magnitude in scales, from $k = 2 \times 10^{-4}$ to $k = 2\,h\,\mathrm{Mpc}^{-1}$, and a wide range of cosmic history, from $z \sim 0$ to 1000, shown in Fig. 1. Taking advantage of the advent of new generation instruments to probe cosmic structure, we re-evaluate the study done in Tegmark & Zaldarriaga (2002). We use the latest data sets available for the Lyα forest 1D power spectrum (SDSS-IV DR14), for the Cosmic Microwave Background temperature anisotropies and polarization measurements (Planck 2018), for the cosmic shear two-point correlation function (DES YR1) and for the galaxy clustering with measurements of the halo power spectrum (SDSS DR7).

On scales of a few Mpc we use measurements of the 1D transmitted flux Lyα power spectrum measured by the BOSS and eBOSS surveys of the SDSS (Chabanier et al. 2018). We follow the general method of Croft et al. (2002) to recover the 3D matter power spectrum from the 1D measurements. However, we improve the determination of the total power $P_\mathrm{m}(k, 0)$ compared to the previous analysis by using a refined differentiation technique, the Total Variation Regularization method proposed in Chartrand (2005), which allows us to significantly reduce the resulting dispersion. On small scales, we also use cosmic shear real-space two-point correlation functions from the DES YR1 data release (Troxel et al. 2017), which undergo the same general treatment as in Tegmark & Zaldarriaga (2002). On scales of tens of Mpc, we use measurements of the halo power spectrum from a sample of LRGs from the SDSS seventh data release. We use the halo bias model from Reid et al. (2010). For scales of hundreds of Mpc we use CMB data with temperature, polarization and lensing reconstruction power spectra measurements (Collaboration et al. 2018a,b).

Except for Lyα that undergoes a specific treatment, we apply the general method of Tegmark & Zaldarriaga (2002) to estimate the amplitudes and uncertainties on the 3D matter power spectrum.

Our work provides a qualitative consistency test of the ΛCDM model. Although we do not perform any thorough quantitative tests, we have computed the χ^2 of the the data points shown in Fig. 1 against our fiducial model, ignoring any covariance between the data points, and using only the error bars in the y-direction. We find $\chi^2 = 117.3$ for 108 degrees of freedom, which is consistent with an expected χ^2 fluctuation to within $1\,\sigma$. We stress that this number is only a very rough quantitative estimate of the consistency, but does at least highlight that no discrepancy is hiding in the residuals of Fig. 1. Our results thus highlight the good agreement of the ΛCDM model with observational data issued by independent experiments, covering a large range of cosmic times and cosmic scales.

ACKNOWLEDGEMENTS

We thank Guillaume Mention for valuable advice on the Total Variation Regularization technique, and Martin White and Benjamin Wallisch for helpful input.

REFERENCES

Abolfathi B., et al., 2018, ApJS, 235, 42
Armengaud E., Palanque-Delabrouille N., Yèche C., Marsh D. J. E., Baur J., 2017, MNRAS , 471, 4606
Baur J., Palanque-Delabrouille N., Yèche C., Magneville C., Viel M., 2016, JCAP, 8, 012
Baur J., Palanque-Delabrouille N., Yèche C., Boyarsky A., Ruchayskiy O., Armengaud É., Lesgourgues J., 2017, JCAP, 12, 013
Bautista J. E., et al., 2017, A&A, 603, A12
Bennett C. L., et al., 2013, ApJS, 208, 20
Blanton M. R., et al., 2017, AJ, 154, 28
Borde A., Palanque-Delabrouille N., Rossi G., Viel M., Bolton J. S., Yèche C., LeGoff J.-M., Rich J., 2014, JCAP, 7, 5
Busca N. G., et al., 2013, Astronomy & Astrophysics, 552, A96
Chabanier S., Palanque-Delabrouille N., Yèche C., et al., 2018, arXiv:1812.03554 [astro-ph]
Chartrand R., 2005, ISRN Applied Mathematics, 2011, Article ID 164564
Collaboration P., et al., 2018a, arXiv:1807.06205 [astro-ph]
Collaboration P., et al., 2018b, arXiv:1807.06210 [astro-ph]
Colless M., et al., 2001, MNRAS , 328, 1039
Croft R. A. C., Weinberg D. H., Katz N., Hernquist L., 1998, The Astrophysical Journal, 495, 44
Croft R. A. C., Weinberg D. H., Bolte M., Burles S., Hernquist L., Katz N., Kirkman D., Tytler D., 2002, The Astrophysical Journal, 581, 20
Dawson K. S., et al., 2016, AJ, 151, 44
Delubac T., et al., 2015, A&A, 574, A59
Hlozek R., et al., 2012, The Astrophysical Journal, 749, 90
Hoekstra H., Yee H. K. C., Gladders M. D., 2002, ApJ , 577, 595
Iršič V., et al., 2017, Phys. Rev. D , 96, 023522
Kirkby D., et al., 2013, JCAP, 3, 024
Lesgourgues J., 2011, preprint, (arXiv:1104.2932)
Lewis A., Challinor A., Lasenby A., 2000, The Astrophysical Journal, 538, 473
McDonald P., et al., 2006, The Astrophysical Journal Supplement Series, 163, 80
Palanque-Delabrouille N., et al., 2015a, JCAP, 2, 45
Palanque-Delabrouille N., et al., 2015b, JCAP, 11, 11
Planck Collaboration et al., 2014, A&A, 571, A16
Planck Collaboration et al., 2018, arXiv:1807.06209 [astro-ph],
Reid B. A., et al., 2010, Monthly Notices of the Royal Astronomical Society, 404, 60
Slosar A., et al., 2011, JCAP, 9, 001
Slosar A., et al., 2013, Journal of Cosmology and Astroparticle Physics, 2013, 026
Tegmark M., Zaldarriaga M., 2002, Physical Review D, 66, 103508
Tegmark M., Zaldarriaga M., 2009, Physical Review D, 79, 083530
The Dark Energy Survey Collaboration 2005, arXiv e-prints, pp astro–ph/0510346
Troxel M. A., et al., 2017, arXiv:1708.01538 [astro-ph]
Yèche C., Palanque-Delabrouille N., Baur J., du Mas des Bourboux H., 2017, JCAP, 6, 047
York D. G., et al., 2000, The Astronomical Journal, 120, 1579
Zaldarriaga M., 1997, Physical Review D, 55, 1822

This paper has been typeset from a TEX/LATEX file prepared by the author.